EUROPEAN ORGANIZATION FOR NUCLEAR RESEARCH

FURTHER EVIDENCE FOR CHARGED INTERMEDIATE VECTOR BOSONS
AT THE SPS COLLIDER

UA1 Collaboration, CERN, Geneva, Switzerland

Aachen[1]-Annecy (LAPP)[2]-Birmingham[3]-CERN[4]-Helsinki[5]-Queen Mary College, London[6]-Paris (Coll. de France)[7]-Riverside[8]-Rome[9]-Rutherford Appleton Lab.[10]-Saclay (CEN)[11]-Vienna[12] Collaboration

G. Arnison[10], A. Astbury[10], B. Aubert[2], C. Bacci[9], G. Bauer[*], A. Bézaguet[4],
R. Bock[4], T.J.V. Bowcock[6], M. Calvetti[4], P. Catz[2], P. Cennini[4],
S. Centro[4], F. Ceradini[4,9], S. Cittolin[4], D. Cline[*], C. Cochet[11], J. Colas[2],
M. Corden[3], D. Dallman[4,12], D. Dau[**], M. DeBeer[11], M. Della Negra[2,4], M. Demoulin[4],
D. Denegri[11], A. Di Ciaccio[9], D. DiBitonto[4], L. Dobrzynski[7], J.D. Dowell[3],
K. Eggert[1], E. Eisenhandler[6], N. Ellis[4], P. Erhard[1], H. Faissner[1], M. Fincke[**],
G. Fontaine[7], R. Frey[8], R. Frühwirth[12], J. Garvey[3], S. Geer[7], C. Ghesquière[7],
P. Ghez[2], K. Giboni[1], W.R. Gibson[6], Y. Giraud-Héraud[7], A. Givernaud[11], A. Gonidec[2],
G. Grayer[10], T. Hansl-Kozanecka[1], W.J. Haynes[10], L.O. Hertzberger[***], C. Hodges[8],
D. Hoffmann[1], H. Hoffmann[4], D.J. Holthuizen[***], R.J. Homer[3], A. Honma[6], W. Jank[4],
G. Jorat[4], P.I.P. Kalmus[6], V. Karimäki[5], R. Keeler[6], I. Kenyon[3], A. Kernan[8],
R. Kinnunen[5], W. Kozanecki[8], D. Kryn[4,7], F. Lacava[9], J.-P. Laugier[11], J.-P. Lees[2],
H. Lehmann[1], R. Leuchs[1], A. Lévêque[11,4], D. Linglin[2], E. Locci[11], J.-J. Malosse[11],
T. Markiewicz[4], G. Maurin[4], T. McMahon[3], J.-P. Mendiburu[7], M.-N. Minard[2],
M. Mohammadi[*], M. Moricca[9], K. Morgan[8], H. Muirhead[+], F. Muller[4], A.K. Nandi[10],
L. Naumann[4], A. Norton[4], A. Orkin-Lecourtois[7], L. Paoluzi[9], F. Pauss[4],
G. Piano Mortari[9], E. Pietarinen[5], M. Pimiä[5], A. Placci[4], J.P. Porte[4],
E. Radermacher[1], J. Ransdell[8], H. Reithler[1], J.-P. Revol[4], J. Rich[11],
M. Rijssenbeek[4], C. Roberts[10], J. Rohlf[4,++], P. Rossi[4], C. Rubbia[4], B. Sadoulet[4],
G. Sajot[7], G. Salvi[6], G. Salvini[9], J. Sass[11], J. Saudraix[11], A. Savoy-Navarro[11],
D. Schinzel[4], W. Scott[10], T.P. Shah[10], D. Smith[8], M. Spiro[11], J. Strauss[12],
J. Streets[3], K. Sumorok[4], F. Szoncso[12], C. Tao[***], G. Thompson[6], J. Timmer[4],
E. Tscheslog[1], J. Tuominiemi[5], B. Van Eijk[***], J.-P. Vialle[4], J. Vrana[7],
V. Vuillemin[4], H.D. Wahl[12], P. Watkins[3], J. Wilson[3], R. Wilson[++], C. Wulz[12],
Y.G. Xie[4], M. Yvert[2], E. Zurfluh[4]

(Submitted to Physics Letters B)

*) University of Wisconsin, Madison, Wisconsin, USA.
**) University of Kiel, Fed. Rep. Germany.
***) NIKHEF, Amsterdam, The Netherlands.
+) Visitor from the University of Liverpool, England.
++) Harvard University, Cambridge, Mass., USA.

ABSTRACT

A sample of 52 Intermediate Vector Boson decays in the $(\nu_e e)$ channel is described. They were produced at the CERN SPS Collider for an integrated luminosity of 0.136 pb^{-1}. Both production and decay properties fit well with expectations from the Standard Model of weak interactions. An improved value for the W mass is given and compared with the previously published value for the Z^0 mass.

1. INTRODUCTION

We have recently reported [1] the observation of five events selected by the presence of an isolated, high transverse momentum electron and the absence of a prominent associated jet activity. The events all exhibited a very large missing transverse energy, interpreted as neutrino emission. The vector momenta of the electron and neutrino were found to be consistent with the assumption of the two-body decay of the type $W \rightarrow e\nu_e$. Since no other background could be found, they were interpreted as evidence for Intermediate Vector Bosons (IVBs). A value for the mass was also given:

$$m_W = (81 \pm 5) \text{ GeV}/c^2 .$$

The experiment has been continued and the sample of events has now considerably increased. The present paper deals with a sample of 52 events. With improved statistics the following conclusions can be drawn:

i) The production kinematics and the event rate agree with the hypothesis of quark-antiquark annihilation in a massive state, $W^{\pm}$.

ii) The decay kinematics favours the two-body decay $W^{\pm} \rightarrow e^{\pm}\nu_e$.

iii) The angular distributions of positive and negative electrons are significantly different. This effect is in agreement with what is expected from a spin-one particle being produced and decaying into fermion-antifermion states with maximal helicity.

iv) The precision in the determination of the mass of the $W^{\pm}$ particle has been considerably improved.

The UA1 detector is a very general purpose apparatus designed to study, as systematically as possible, the large-angle phenomenology of $\bar{p}p$ collisions at $\sqrt{s} = 540$ GeV. The apparatus and the data-taking conditions are essentially unchanged from the work already reported, and we refer the reader to Ref. 1 for more details. The main features of the UA1 detector for the present investigations are the following:

i) Electron detection. The electron energy is determined by the energy sampled by lead scintillator shower counters 27 radiation lengths deep, and the absence of significant leakage beyond these. The energy resolution is approximately $\Delta E_{rms} = 0.16 \sqrt{E}$, where all energies are in GeV. Additional uncertainties are due to fluctuations in the absolute energy calibration for each counter element.

ii) Neutrino detection. The presence of neutrino emission is signalled by an apparent lack of momentum conservation in the two components transverse to the beam. This unique feature of the UA1 detector is due to the complete solid-angle coverage of calorimeters down to 0.2° from the direction of the beams. The accuracy in each component of missing transverse energy is $0.4 \sqrt{E_T}$, where E_T is the scalar sum of energy depositions in the transverse plane and all units are GeV.

iii) Momentum analysis and charged particle determination. This is performed with accurate curvature measurement by the central detector, a large drift-chamber volume surrounding the crossing point and operated in a homogeneous 7 kG magnetic field. The central detector is also used to determine the over-all topology of the event and, in particular, the isolation criteria for the electron track.

Recently we have also reported [2] the observation of high invariant mass muon and electron pairs, due to the decay of a narrow, massive neutral particle. These events have been interpreted as due to the Z^0 particle, the neutral partner of the $W^{\pm}$'s. Since both $W^{\pm}$ and Z^0 are observed simultaneously in our detector, relative comparisons between mass values and cross-sections will be given.

2. EVENT SELECTION

Results are based on an integrated luminosity of 0.136 pb^{-1}, which is corrected for dead-time and other similar losses and which includes the exposure for which results have been previously reported [1]. The trigger selection used throughout the investigation required the presence of an electromagnetic cluster at angles larger than 5°, with transverse energy in excess of 10 GeV. After on-line filtering and complete off-line reconstruction, about 1.5×10^5 events had at least one electromagnetic (e.m.) cluster with $E_T > 15$ GeV. By requiring the presence of an associated, isolated [1]

track with p_T > 7 GeV/c in the central detector, we reduced the sample by a factor of about 100. Next, a maximum energy deposition (leakage) of 600 MeV is allowed in the hadron calorimeter cells after the e.m. counters, leading to a sample of 346 events. We then classify events according to whether there is a prominent jet activity. We find that in 291 events there is a clearly visible jet [3] within an azimuthal angle cone $|\Delta\phi|$ < 30° opposite to the "electron" track. These events are strongly contaminated by jet-jet events in which one jet fakes the electron signature and must be rejected. We are left with 55 events without any jet or with a jet not back-to-back with the "electron" within 30°.

The bulk of these events is characterized by the presence of neutrino emission, signalled by a significant missing energy (see fig. 1). According to the experimental energy resolutions, at most the three lowest missing energy events are compatible with no neutrino emission. They are excluded by the cut E_T^{miss} > 15 GeV. We are then left with 52 events. These events have a very clean electron signature (figs. 2a-c) and a perfect matching between the point of electron incidence and the centroid in the shower detectors, further supporting the absence of composite overlaps of a charged track and neutral π^0's expected from jets.

In order to ensure the best accuracy in the electron energy determination, only events in which the electron track hits the electromagnetic detectors more than ±15° away from their top and bottom edges have been retained. The sample is then reduced to 43 events.

We have estimated, in detail, the possible sources of background coming from ordinary hadronic interactions with the help of a sample of isolated hadrons at large transverse momenta and we conclude that they are negligible (< 0.5 events). For more details on background we refer the reader to ref. 1. We may, however, detect some background events from other decays of the W, namely

$$W \rightarrow \tau\nu_\tau \qquad \text{(< 0.5 events)}$$
$$ \hookrightarrow \pi^\pm(\pi^0)\nu_\tau$$

or

$$W \rightarrow \tau \nu_\tau \qquad (\simeq 2 \text{ events})$$
$$ \hookrightarrow e \nu_e \nu_\tau$$

These events are expected to contribute only at the low p_T part of the electron spectrum and they can be eliminated in a more restrictive sample.

3. ORIGIN OF THE ELECTRON-NEUTRINO EVENTS

We proceed to a detailed investigation of the events in order to elucidate their physical origin. The large missing energy observed in all events is interpreted as being due to the emission of one or of several non-interacting neutrinos. A very strong correlation in angle and energy is observed (in the plane normal to the colliding beams, where it can be determined accurately), with the corresponding electron quantities, in a characteristic back-to-back configuration expected from the decay of a massive, slow particle (figs. 3a and b). This suggests a common physical origin for the electron and for one or several neutrinos. In order to understand better the transverse motion of the electron-neutrino(s) system one can study the experimental distribution of the resultant transverse momentum $p_T^{(W)}$ obtained by adding neutrino(s) and electron momenta (fig. 4). The average value is $p_T^{(W)}$ = 6.3 GeV/c. Five events which have a visible jet have also the highest values of $p_T^{(W)}$. Transverse momentum balance can be almost exactly restored if the vector momentum of the jet is added. The experimental distribution is in good agreement with the many theoretical expectations from QCD for the production of a massive state via the Drell-Yan quark-antiquark annihilation [4]. The small fraction (10%) of events with a jet are then explained as hard gluon bremsstrahlung in the initial state [5].

Several different hypotheses on the physical origin of the events can be tested by looking at kinematical quantities constructed from the transverse variables of the electron and the neutrino(s). We retain here two possibilities, namely (i) the two-body decay of a massive particle into the electron and one neutrino, $W \rightarrow e\nu_e$; and (ii) the three-body decay into two, or possibly more, neutrinos and the electron. One can see from figs. 5a and b that hypothesis (i)

is strongly favoured. At this stage, the experiment cannot distinguish between one or several closely spaced massive states.

4. DETERMINATION OF THE INVARIANT MASS OF THE $(e\nu_e)$ SYSTEM

A (common) value of the mass m_W can be extracted from the data in a number of ways, namely:

i) It can be obtained from the inclusive transverse-momentum distribution of the electrons (fig. 5a). The drawback of this technique is that the transverse momentum of the W particle must be known. Taking the QCD predictions [4], in reasonable agreement with experiment, we obtain $m_W = (80.5 \pm 0.5)$ GeV/c^2.

ii) We can define a transverse mass variable, $m_T^2 = 2p_T^{(e)} p_T^{(\nu)} (1 - \cos \phi)$, with the property $m_T \leq m_W$, where the equality holds only for events with no longitudinal momentum components. Fitting fig. 5b to a common value of the mass can be done almost independently of the transverse motion of the W particles, $m_W = (80.3^{+0.4}_{-1.3})$ GeV/c^2. It should be noted that the lower part of the distribution in $m_T^{(W)}$ may be slightly affected by $W \rightarrow \tau\nu_\tau$ decays and other backgrounds.

iii) We can define an enhanced transverse mass distribution, selecting only events in which the decay kinematics is largely dominated by the transverse variable with the simple cuts $p_T^{(e)}$, $p_T^{(\nu)} > 30$ GeV/c. The resultant distribution (fig. 5c) shows then a relatively narrow peak, at approximately 76 GeV/c^2. Model-dependent corrections contribute now only to the difference between this average mass value and the fitted m_W value, $m_W = (80.9 \pm 1.5)$ GeV/c^2. An interesting upper limit to the width of the W can also be derived from the distribution, namely $\Gamma_W \leq 7$ GeV/c^2 (90% confidence level).

The three mass determinations give very similar results. We prefer to retain the result of method (iii), since we believe it is the least affected by systematic effects, even if it gives the largest statistical error. Two important contributions must be added to the statistical errors:

i) Counter-to-counter energy calibration differences. They can be estimated indirectly from calibrations of several units in a beam of electrons; or, and more

reliably, by comparing the average energy deposited by minimum bias events recorded periodically during the experiment. From these measurements we find that the r.m.s. spread does not exceed 4%. In the determination of the W mass this effect is greatly attenuated, to the point of being small compared to statistical errors, since many different counter elements contribute to the event sample.

ii) Calibration of the absolute energy scale. This has been performed using a strong ^{60}Co source in order to transfer test-beam measurements to the counters in the experiment. Several small effects introduce uncertainties in such a procedure, some of which are still under investigation. At the present stage we quote an over-all error of ±3% on the energy scale of the experiment. Of course this uncertainty influences *both* the $W^{\pm}$ and Z^0 mass determinations by the same multiplicative correction factor.

5. LONGITUDINAL MOTION OF THE W PARTICLES

Once the decay reaction $W \rightarrow e\nu_e$ has been established, the longitudinal momentum of the electron-neutrino system can be determined with a two-fold ambiguity for the unmeasured longitudinal component of the neutrino momentum. The over-all information of the event can be used to establish momentum and energy conservation bounds in order to resolve this ambiguity in 70% of the cases. Most of the remaining events have solutions which are quite close, and the physical conclusions are nearly the same for both solutions. The fractional beam energy x_W carried by the W particle is shown in fig. 6a and it appears to be in excellent agreement with the hypothesis of W production in $q\bar{q}$ annihilation [7]. Using the well-known relations $x_W = x_p - x_{\bar{p}}$ and $x_p \cdot x_{\bar{p}} = m_W^2/s$, we can determine the relevant parton distributions in the proton and antiproton. One can see that the distributions are in excellent agreement with the expected x distributions for quarks and antiquarks respectively in the proton and antiproton (fig. 6b and c). Contributions of the u and d quarks can also be neatly separated, by looking at the charges of produced W events, since $(u\bar{d}) \rightarrow W^+$ and $(\bar{u}d) \rightarrow W^-$ (figs. 6d and e).

6. EFFECTS RELATED TO THE SIGN OF THE ELECTRON CHARGE

The momentum of the electrons is measured by their curvature in the magnetic field of the central detector. Out of the 52 events, 24 (14) have a negative (positive) charge assignment; 14 events have a track topology which makes charge determination uncertain. Energy determinations by calorimetry and momentum measurements are compared in fig. 7a, and they are, in general, in quite reasonable agreement with what is expected from isolated high-energy electrons. A closer examination can be performed, looking at the difference between curvature observed and expected from the calorimeter energy determination, normalized to the expected errors (fig. 7b). One can observe a significant deviation from symmetry (corresponding to $p < E$), which can be well understood once the presence of radiative losses of the electron track (internal and external bremsstrahlung), is taken into account [6].

Weak interactions should act as a longitudinal polarizer of the W particles since quarks (antiquarks) are provided by the proton (antiproton) beam. Likewise decay angular distributions from a polarizer are expected to have a large asymmetry, which acts as a polarization analyser. A strong backward-forward asymmetry is therefore expected, in which electrons (positrons) prefer to be emitted in the direction of the proton (antiproton). In order to study this effect independently of W-production mechanisms, we have looked at the angular distribution of the emission angle θ^* of the electron (positron) with respect to the proton (antiproton) direction in the W centre of mass. Only events with no reconstruction ambiguity can be used. It has been verified that this does not bias the distribution in the variable $\cos \theta^*$. According to expectations of V − A theory the distribution should be of the type $(1 + \cos \theta^*)^2$, in excellent agreement with the experimental data (fig. 8).

More generally it has been shown by Jacob [8] that for a particle of arbitrary spin J one expects:

$$\langle \cos \theta^* \rangle = \frac{\langle \lambda \rangle \langle \mu \rangle}{J(J+1)} \, ,$$

where $\langle \mu \rangle$ and $\langle \lambda \rangle$ are, respectively, the global helicity of the production system $(u\bar{d})$ and of the decay system $(e\bar{\nu})$. For V − A one then has $\langle \lambda \rangle = \langle \mu \rangle = -1$, J = 1, leading to the maximal value $\langle \cos \theta^* \rangle = 0.5$. For J = 0 one obviously expects $\langle \cos \theta^* \rangle = 0$ and for any other spin value J ≥ 2, $\langle \cos \theta^* \rangle \leq 1/6$. Experimentally, we find $\langle \cos \theta^* \rangle = 0.4 \pm 0.1$, which supports *both* the J = 1 assignment *and* maximal helicity states at production and decay. Note that the choice of sign $\langle \mu \rangle = \langle \lambda \rangle = = \pm 1$ cannot be separated, i.e. right− and left−handed currents both at production and decay cannot be resolved without a polarization measurement.

7. TOTAL CROSS−SECTION AND LIMITS TO HIGHER MASS W's

The integrated luminosity of the experiment was 136 nb^{-1} and it is known to about ± 15% uncertainty. In order to get a clean W → ev_e sample we select 47 events with $p_T^{(e)}$ > 20 GeV/c. The W → τv_τ contamination in the sample is estimated to be 2 ± 2 events. The event acceptance is estimated to be 0.65, due primarily to: i) the $p_T^{(e)}$ > 20 GeV/c cut (0.80); ii) the jet veto requirement within $\Delta\phi$ = ± 30° (0.96 ± 0.02); iii) the electron−track isolation requirement (0.90 ± 0.07); and iv) the acceptance of events due to geometry (0.94 ± 0.03). The cross−section is then:

$$(\sigma \cdot B)_W = 0.53 \pm 0.08 \, (\pm 0.09) \text{ nb} \ ,$$

where the last error takes into account systematic errors. This value is in excellent agreement with the expectations of the Standard Model [7] $(\sigma \cdot B)_W = 0.39$ nb.

No event with $p_T^{(e)}$ or $p_T^{(v)}$ in excess of the expected distribution for W → ev events has been observed. This result can be used in order to set a limit to the possible existence of very massive W−like objects decaying into electron−neutrino pairs. We find $(\sigma \cdot B)_{W_1} \leq 30$ pb at 90% confidence level, corresponding to m_{W_1} > 170 GeV/c^2, if standard couplings and quark distributions are used to evaluate the cross−sections.

8. COMPARISON BETWEEN CHARGED AND NEUTRAL
   INTERMEDIATE VECTOR BOSON MASSES

The charged vector boson mass given in the present work is

$$m_{W^\pm} = (80.9 \pm 1.5) \text{ GeV/c}^2 \quad \text{(statistical errors only)}$$

to which a 3% energy scale uncertainty must be added. In a recent paper [2] we
have reported a preliminary value for the Z^0 mass, $m_{Z^0} = (95.1 \pm 2.5) \text{ GeV/c}^2$. Since
then the calibration work has been completed and a new mass value is now given with
somewhat smaller errors:

$$m_{Z^0} = (95.6 \pm 1.4) \text{ GeV/c}^2 \quad \text{(statistical errors only)}$$

to which the same scale uncertainty as for the $W^\pm$ applies. The quoted error in-
cludes: i) the natural width of the Z^0 peak, which is found to be $\Gamma < 8.5 \text{ GeV/c}^2$
(90% confidence level), ii) the experimental resolution of counters, and iii) the
r.m.s. spread between calibration constants of individual elements. In fig. 9a
we have plotted m_Z against m_W. The elliptical shape of the errors reflects the
uncertainty in the energy scale. One can see that there is excellent agreement
with the expectations of the SU(2) $\otimes$ U(1) Standard Model [9]. One can also deter-
mine the classic parameters:

$$\sin^2 \theta_W = \left(\frac{38.5 \text{ GeV/c}^2}{m_W} \right) = 0.226 \pm 0.008 \ (\pm 0.014) \ ,$$

$$\rho = \frac{m_W^2}{m_Z^2 \cos^2 \theta_W} = 0.925 \pm 0.05 \ ,$$

where the number in parentheses is due to systematic errors. The result is shown
in fig. 9b, again in good agreement with expectations and published results [10].

REFERENCES AND FOOTNOTES

[1] G. Arnison et al. (UA1 Collaboration), Phys. Lett. 122B (1983) 103.

See also the corresponding result by the UA2 Collaboration: G. Banner et al., Phys. Lett. 122B (1983) 476.

[2] G. Arnison et al. (UA1 Collaboration), Phys. Lett. 126B (1983) 398.

The UA2 Collaboration has reported similar results in July at the 1983 Europhysics Conference, Brighton, UK, to be published in the Proceedings.

[3] For the definition of a jet according to UA1, see for instance J. Sass and V. Vuillemin, papers presented at the Rencontres de Moriond, La Plagne (1983). We require a jet with transverse energy $E_T \geq 10$ GeV.

[4] F. Halzen and W. Scott, Phys. Letters 78B (1978) 318.

P. Aurenche and R. Kinnunen, Annecy preprint LAPP-TH-78 (June 1983).

A. Nakamura, G. Pancheri and Y. Srivastava, Frascati preprint LNF-83/43 (R) (June 1983).

P. Chiappetta and M. Greco, Frascati preprint LNF-83-44 (June 1983).

[5] P. Aurenche and J. Lindfors, Nucl. Phys. B185 (1981) 274.

[6] F. Berends et al., Nucl. Phys. B202 (1982) 63, and private communications.

[7] F.E. Paige and S.D. Protopopescu, ISAJET program, BNL 29777 (1981). All cross-sections are calculated in the leading log approximation, assuming $SU(2) \times U(1)$.

[8] M. Jacob, to be published. We thank Professor M. Jacob for very helpful comments on the subject.

[9] S.L. Glashow, Nucl. Phys. 22 (1961) 579.

S. Weinberg, Phys. Rev. Lett. 19 (1967) 1264.

A. Salam, Proc. 8th Nobel Symposium, Aspenäsgården, 1968 (Almqvist and Wiksell, Stockholm, 1968), p. 367.

For latest details, see for instance C. Rubbia, 1983 Europhysics Conference, Brighton, UK, 1983 (to be published).

[10] J.E. Kim et al., Rev. Mod. Phys. 53 (1981) 211.

Figure captions

Fig. 1 : The distribution of the missing transverse energy for those events in which there is a single isolated electron with $E_T > 15$ GeV, and no co-planar jet activity. The curve represents the resolution function for no missing energy normalized to the three lowest missing-energy events.

Fig. 2 : Distributions showing the quality of the electron signature:

a) The energy deposition in the hadron calorimeter cells behind the 27 radiation lengths (r.l.) of the e.m. shower detector.

b) The fraction of the electron energy deposited in the fourth sampling (6 r.l. deep, after 18 r.l. convertor) of the e.m. shower detector. The curve is the expected distribution from test-beam data.

c) As distribution (b) but for the first sampling of the e.m. shower detector (first 6 r.l.).

Fig. 3 : a) Two-dimensional plot of the transverse components of the missing energy (neutrino momentum). Events have been rotated to bring the electron direction pointing along the vertical axis. The striking back-to-back configuration of the electron-neutrino system is apparent.

b) Correlation between the electron and neutrino transverse energies. The neutrino component along the electron direction is plotted against the electron transverse energy.

Fig. 4 : The transverse-momentum distribution of the W derived from our events using the electron and missing transverse-energy vectors. The highest $p_T^{(W)}$ events have a visible jet (shown in black in the figure). The data are compared with the theoretical predictions of Halzen et al. for W production (a) without $\left[O(\alpha_s)\right]$ and (b) with QCD smearing; and predictions by (c) Aurenche et al., and (d) Nakamura et al. (see ref. 4).

Fig. 5 : a) The electron transverse-energy distribution. The two curves show the results of a fit of the enhanced transverse mass distribution to the hypothesis $W \rightarrow e\nu$ and $X \rightarrow e\nu\nu$. The first hypothesis is clearly preferred.

Fig. 5 : b) The distribution of the transverse mass derived from the measured electron and neutrino vectors. The two curves show the results of a fit to the hypothesis $W \rightarrow e\nu$ and $X \rightarrow e\nu\nu$.

c) The enhanced electron-neutrino transverse-mass distribution (see text). The two curves show the results of a fit to the hypotheses $W \rightarrow e\nu$ and $X \rightarrow e\nu\nu$.

Fig. 6 : a) The fractional beam energy x_W carried by the W. The curve is the prediction obtained by assuming the W has been produced by $q\bar{q}$ fusion [7]. Note that in general there are two kinematic solutions for x_W (see text), which are resolved in 70% of the events by consideration of the energy flow in the rest of the event. Where this ambiguity has been resolved the preferred kinematic solution has been the one with the lowest x_W. In the 30% of the events where the ambiguity is not resolved the lowest x_W solution has therefore been chosen.

b) The x-distribution of the proton quarks producing the W by $q\bar{q}$ fusion. The curve is the prediction assuming $q\bar{q}$ fusion [7].

c) The same as (b) for the antiproton quarks.

d) The same as (b) but for u $(\bar{u})$ quarks in the proton (antiproton).

e) The same as (b) but for d $(\bar{d})$ quarks in the proton (antiproton).

Fig. 7 : a) 1/E plotted against Q/p_{CD} where E is the electron energy determined by the calorimeter, p_{CD} the momentum determined from the curvature of the central detector track, and Q the charge of the track.

b) (1/E − 1/p) normalized by the error on the determination of this quantity. The curve is a Monte Carlo calculation, in which radiative losses due to internal and external bremsstrahlung have been folded with the experimental resolution [6].

Fig. 8 : The angular distribution of the electron emission angle θ^* in the rest frame of the W after correction for experimental acceptance. Only those events in which the electron charge is determined and the kinematic ambiguity (see text) has been resolved have been used. The later requirement has been corrected for in the acceptance calculation.

Fig. 9 : a) m_Z plotted against m_W determined by the UA1 experiment. The elliptical error curves reflect the uncertainty in the energy scale at the 68% and 90% confidence levels. The heavy curve shows the Standard Model prediction for $\rho = 1$ as a function of the Intermediate Vector Boson (IVB) masses.

b) ρ plotted against $\sin^2 \theta_W$ as determined from the measurement of the IVB masses. The 68% and 90% confidence level limits are shown.

55 EVENTS

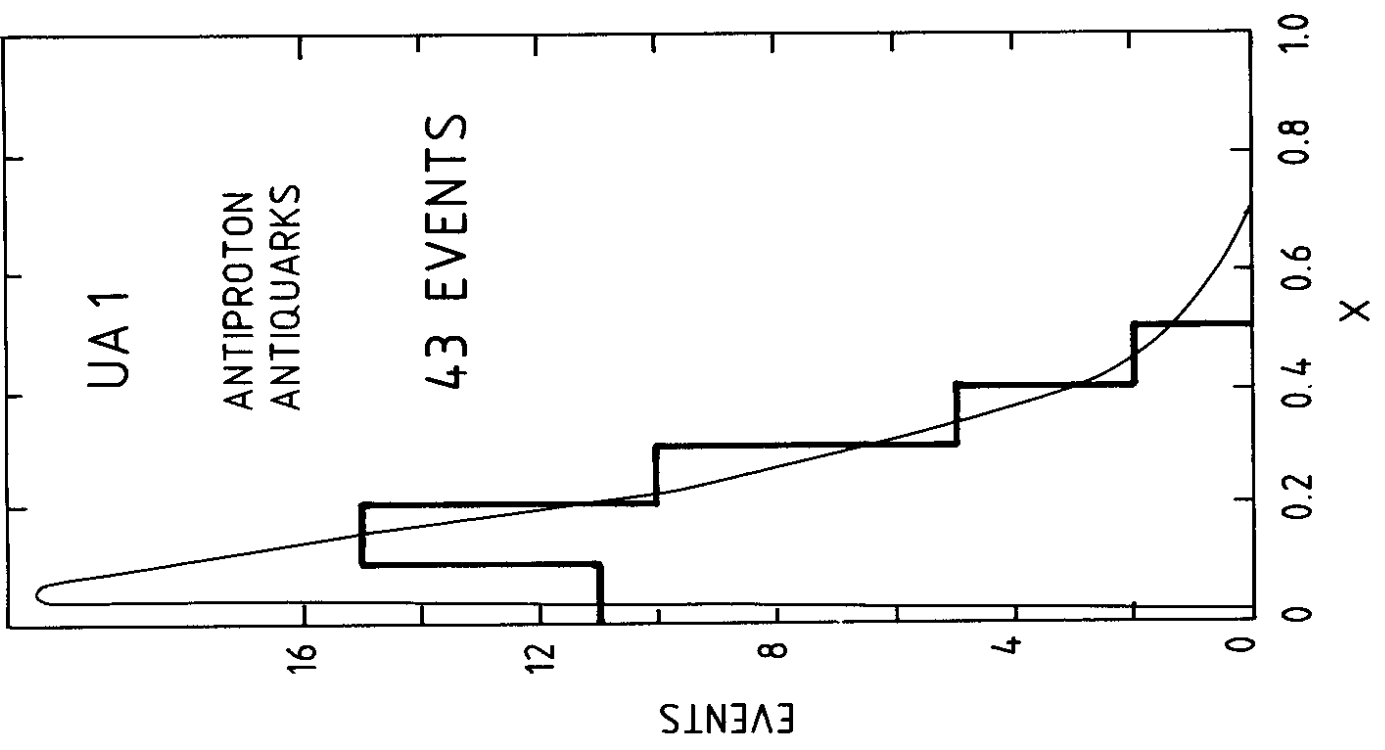Events / 4 GeV

Missing transverse energy (GeV)
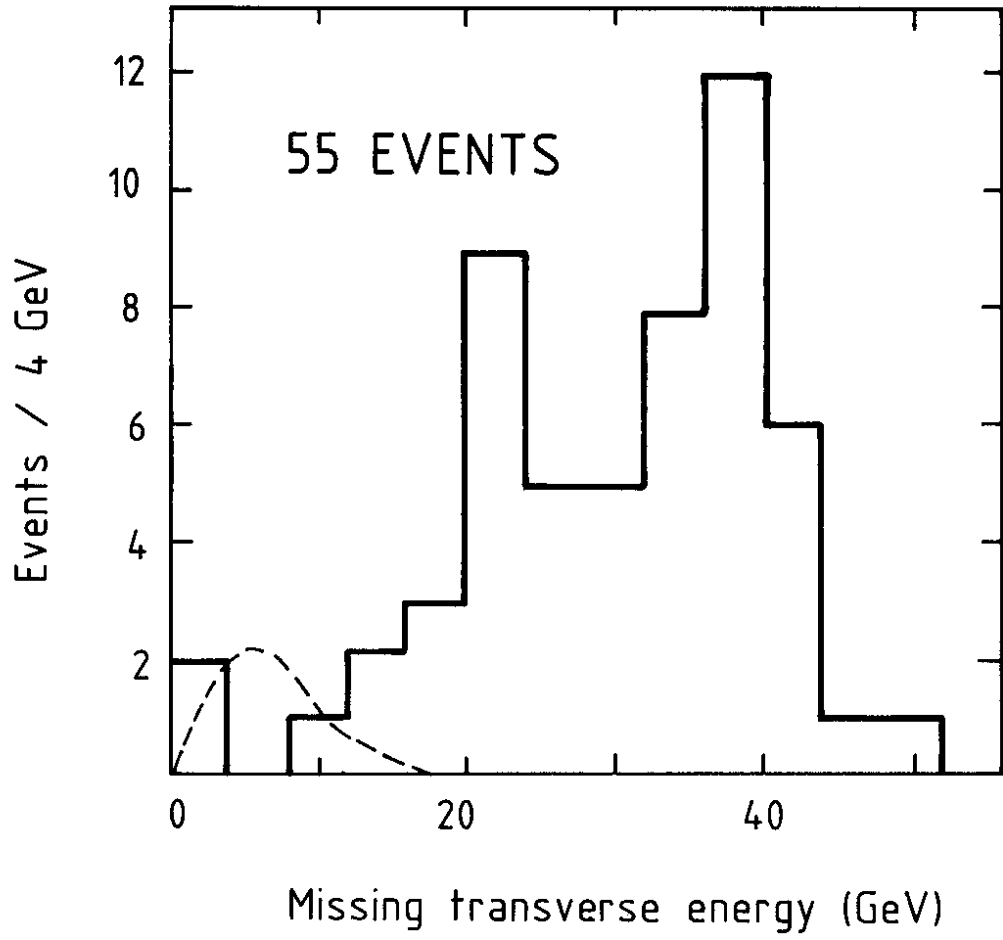
Fig. 1
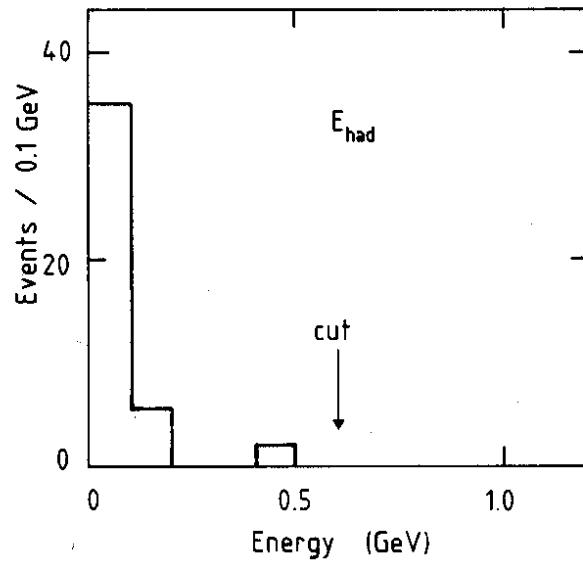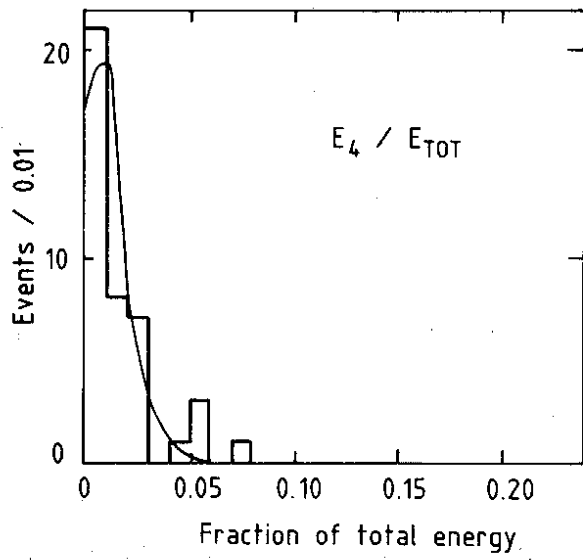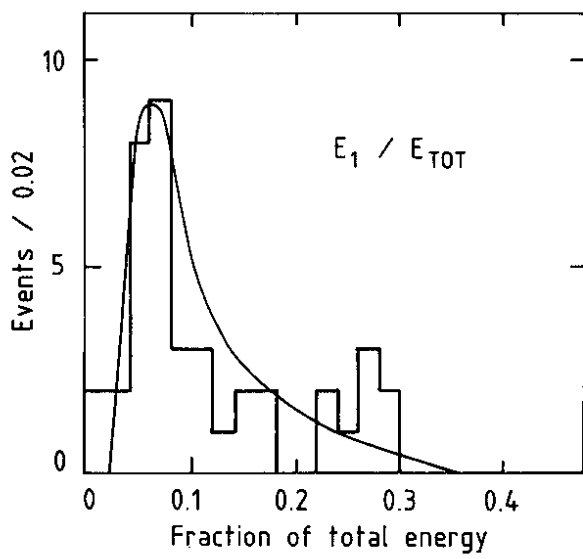
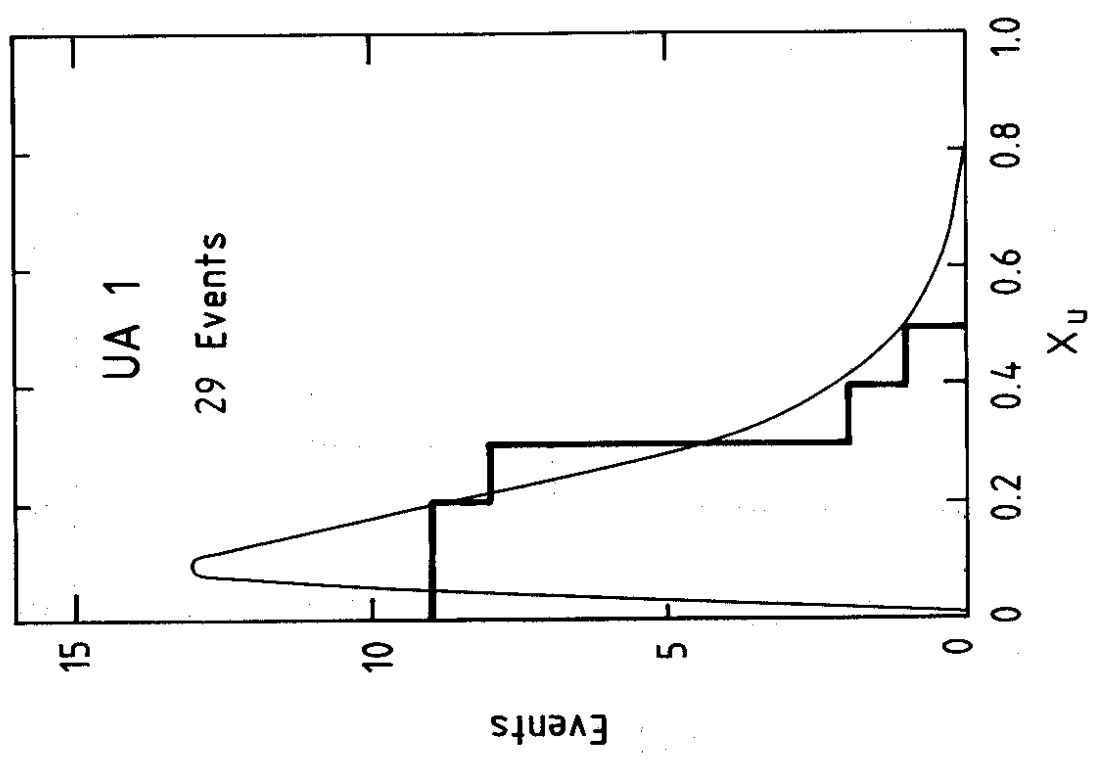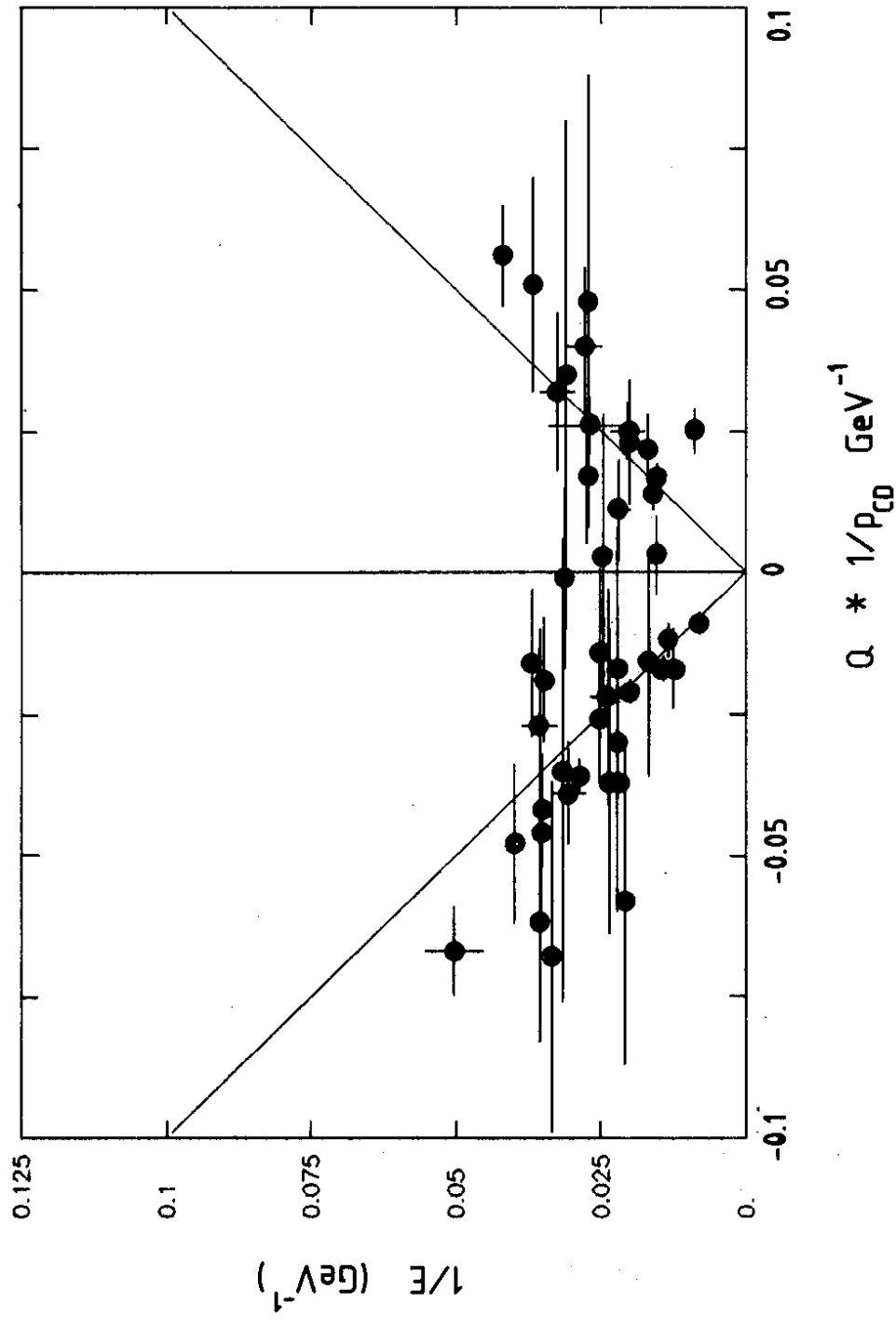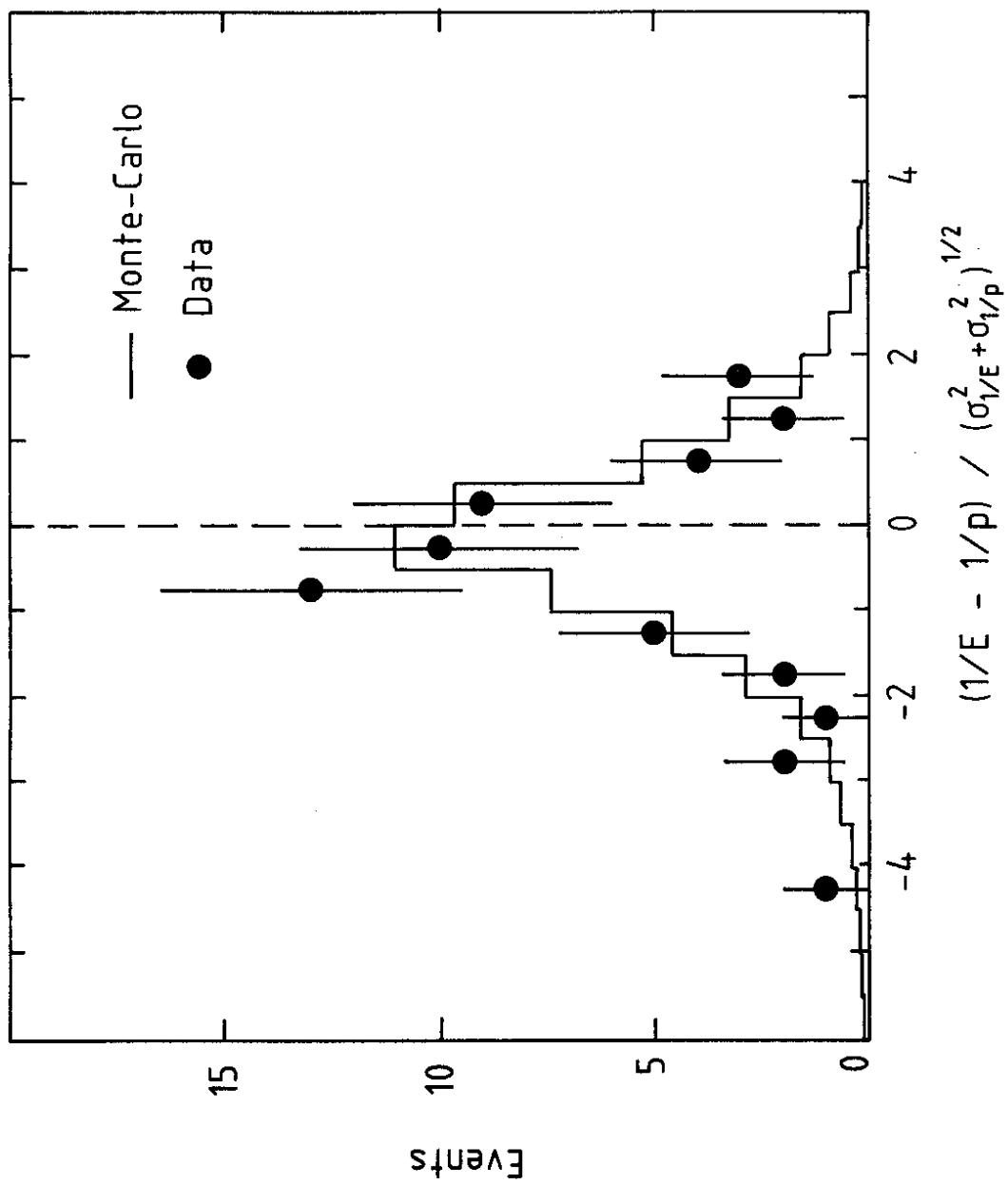Fig. 2
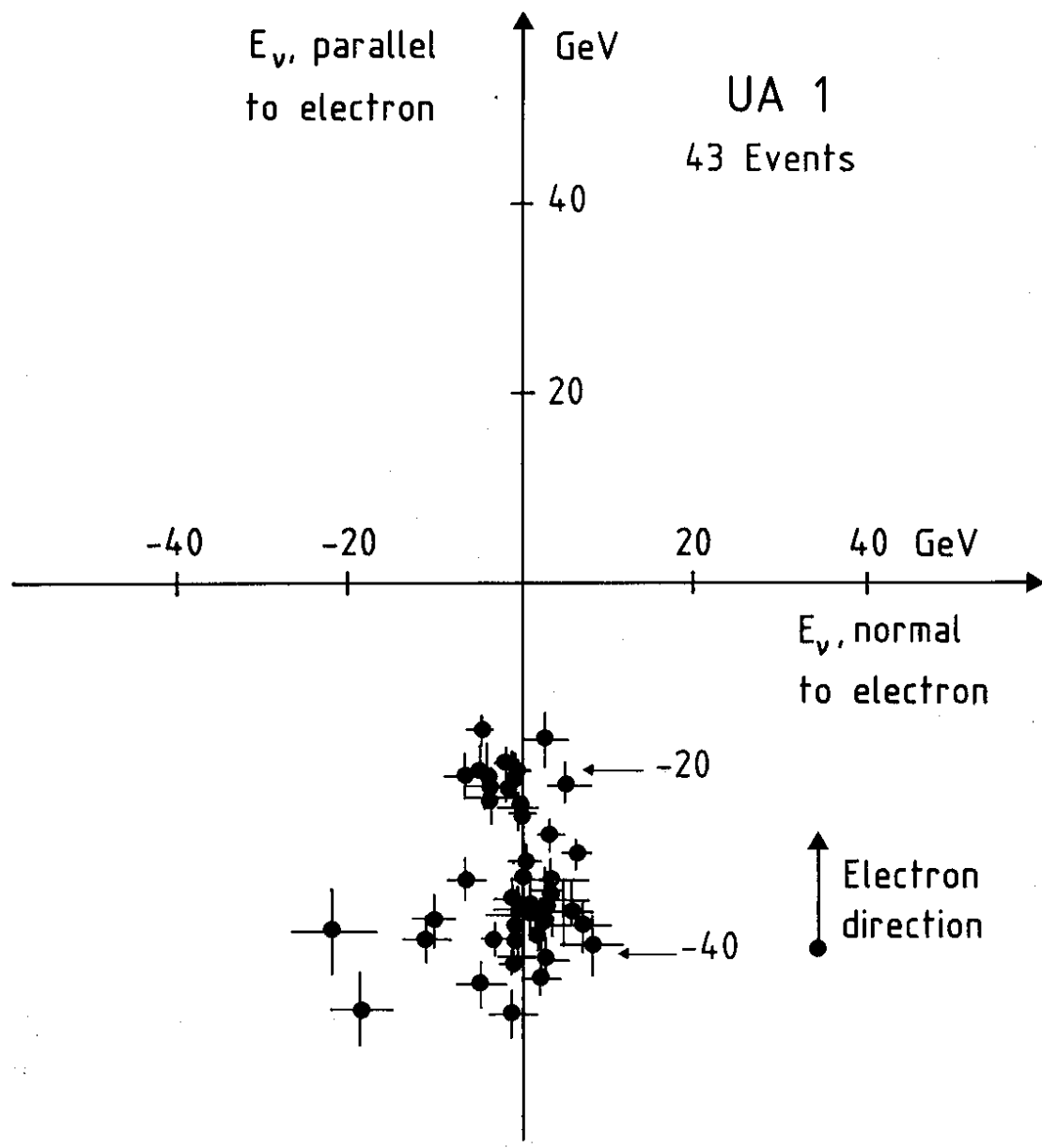
Fig. 3a
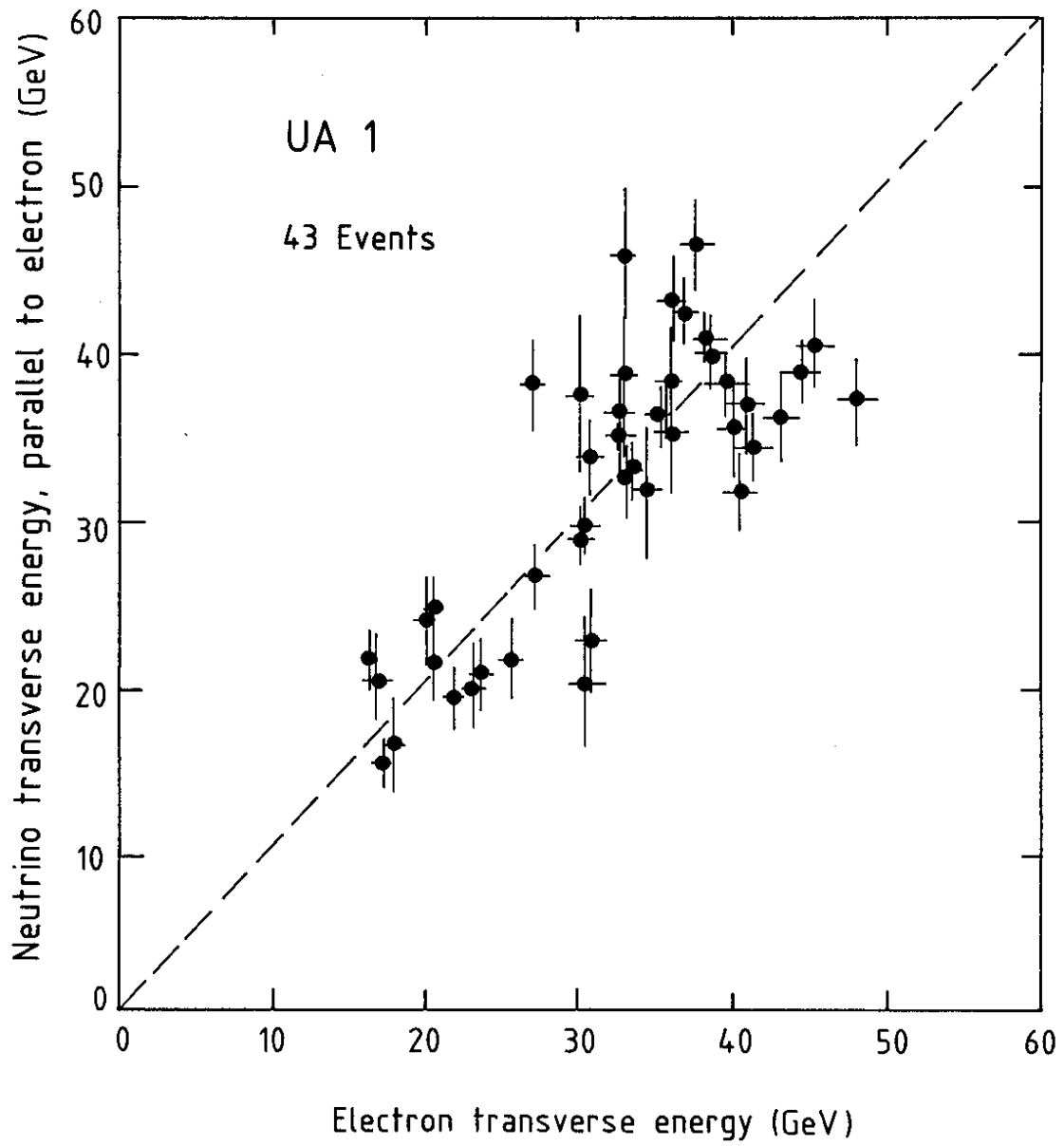
Fig. 3b
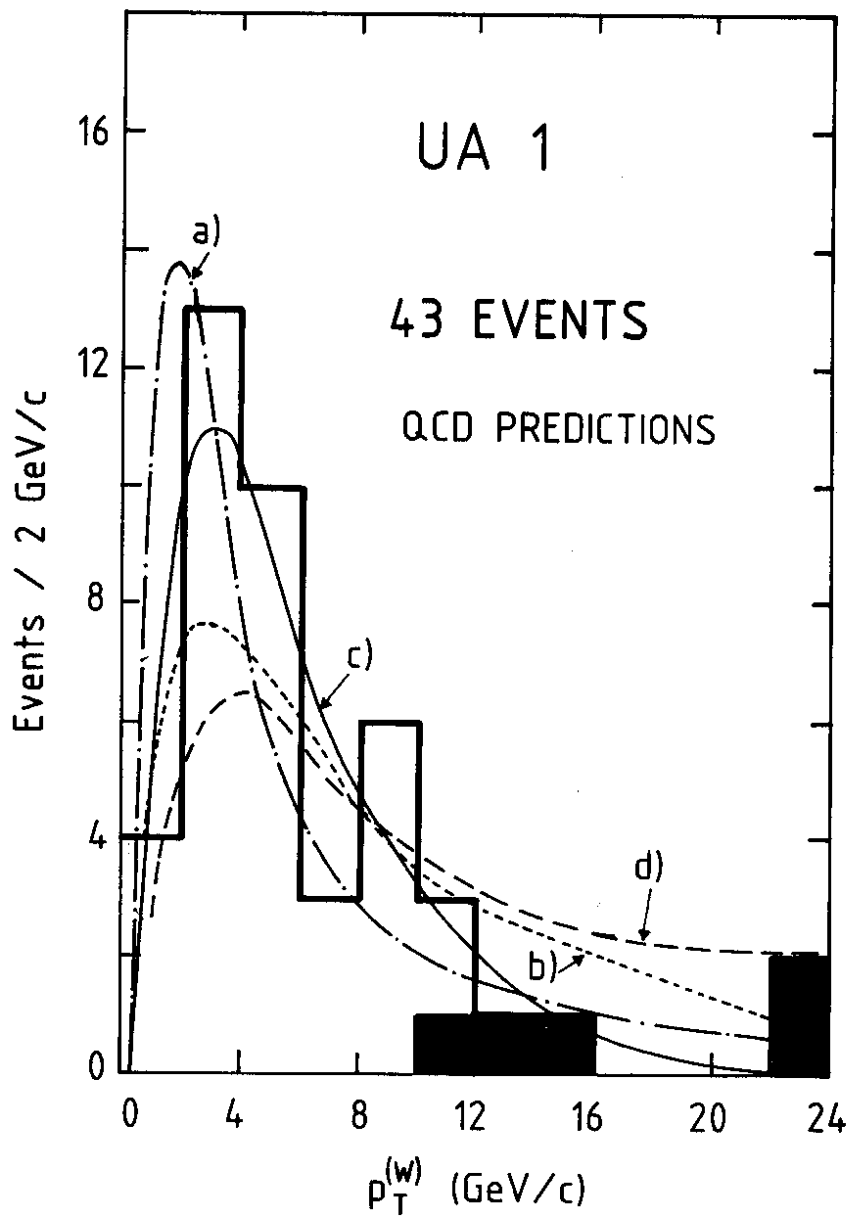
Fig. 4
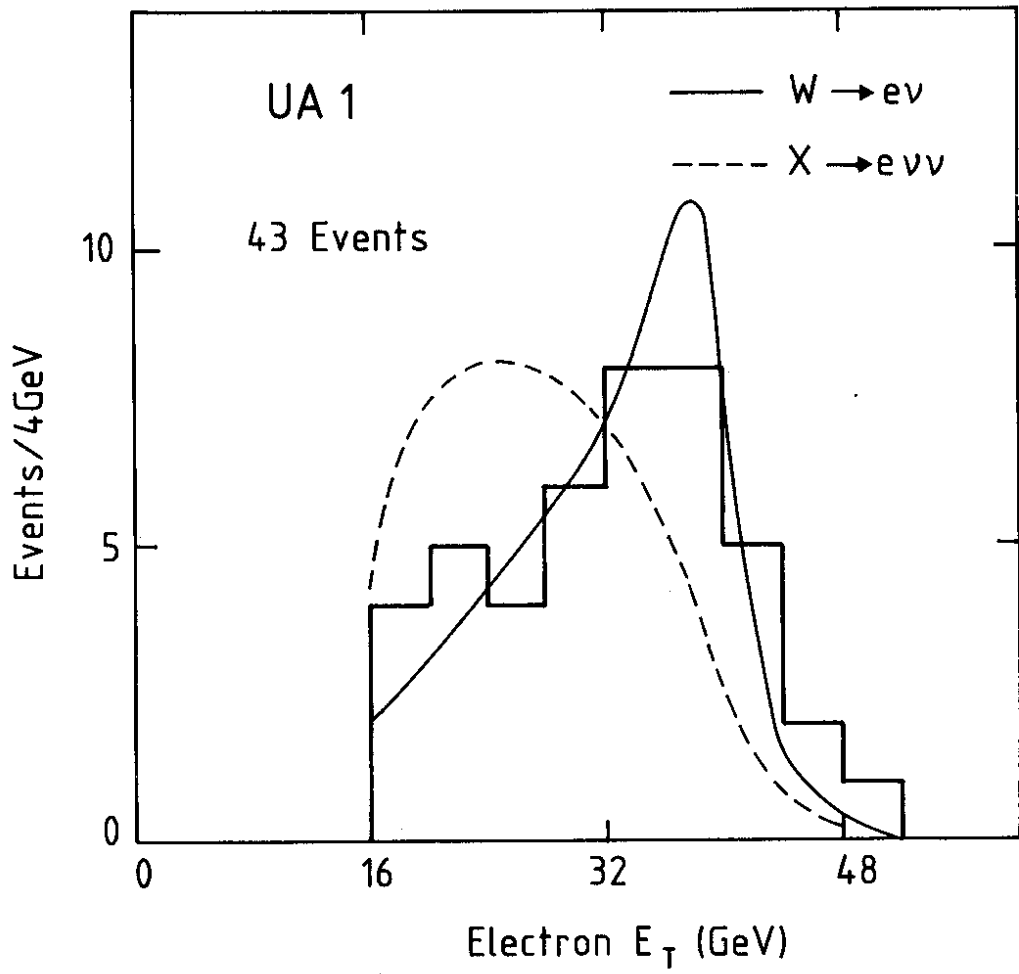
Fig. 5a

Fig. 5b

Fig. 5c

Fig. 6a

Fig. 6b

Fig. 6c

UA 1

29 Events

Events

15

10

5

0

0   0.2   0.4   0.6   0.8   1.0

X_d

Fig. 6e

UA 1

29 Events

Events

15

10

5

0

0   0.2   0.4   0.6   0.8   1.0

X_u

Fig. 6d

Fig. 7a

Monte-Carlo

● Data

Events

$(1/E - 1/p) / (\sigma_{1/E}^2 + \sigma_{1/p}^2)^{1/2}$

Fig. 7b

Fig. 8

$$\sin^2\theta \equiv 1 - (m_W / m_z)^2$$

Fig. 9a

$$\sin^2\theta_W \equiv \left(\frac{38.5 \ \text{GeV}/c^2}{m_W} \right)^2$$

$$\rho \equiv \frac{m_W^2}{m_Z^2 \ \cos^2\theta_W}$$

Fig. 9b